

UC Irvine

UC Irvine Previously Published Works

Title

Micropyramid-patterned, oxygen-permeable bottomed dish for high density culture of pancreatic islets

Permalink

<https://escholarship.org/uc/item/6nz6r7xc>

Journal

Biofabrication, 15(1)

ISSN

1758-5082

Authors

Myrick, Ryan J
Shang, Kuang-Ming
Betts, Jonathan F
[et al.](#)

Publication Date

2023

DOI

10.1088/1758-5090/aca79a

Copyright Information

This work is made available under the terms of a Creative Commons Attribution License, available at <https://creativecommons.org/licenses/by/4.0/>

Peer reviewed



PAPER

Micropyramid-patterned, oxygen-permeable bottomed dish for high density culture of pancreatic islets

To cite this article: Ryan J Myrick *et al* 2023 *Biofabrication* **15** 015018

View the [article online](#) for updates and enhancements.

You may also like

- [Experimental studies on a novel roll-to-roll powder hot embossing for large-area fabrication of micropyramid arrays on polymers](#)
Peiyun Yi, Yujun Deng, Yunyi Shu et al.
- [Selection of polymers for application in scaffolds applicable for human pancreatic islet transplantation](#)
Alexandra M Smink, Bart J de Haan, Genaro A Paredes-Juarez et al.
- [Mathematical modeling of gap junction coupling and electrical activity in human - cells](#)
Alessandro Loppini, Matthias Braun, Simonetta Filippi et al.

Biofabrication



PAPER




Micropyramid-patterned, oxygen-permeable bottomed dish for high density culture of pancreatic islets

RECEIVED
25 June 2022

REVISED
18 November 2022

ACCEPTED FOR PUBLICATION
30 November 2022

PUBLISHED
20 December 2022

Ryan J Myrick^{1,5} , Kuang-Ming Shang^{2,5} , Jonathan F Betts¹, Nelson Gonzalez³, Jeffrey Rawson³, Kenji Izumi⁴, Naoya Koba⁴, Takanori Tsuchiya⁴, Hiroyuki Kato³, Keiko Omori³, Fouad Kandeel³, Yoko Mullen³, Yu-Chong Tai², Elliot Botvinick¹ and Hirotake Komatsu^{3,*} 

¹ Department of Surgery and Biomedical Engineering, University of California, Irvine. 5200 Engineering Hall, Irvine, CA 92697, United States of America

² Department of Medical Engineering, California Institute of Technology, 1200 E. California Blvd., MC 136-93, Pasadena, CA 91125, United States of America

³ Department of Translational Research & Cellular Therapeutics, Arthur Riggs Diabetes & Metabolism Research Institute of City of Hope, 1500 E. Duarte Rd., Duarte, CA 91010, United States of America

⁴ Tokai Hit, 306-1 Gendojicho, Fujinomiya, Shizuoka 418-0074, Japan

⁵ These authors contributed equally to this work.

* Author to whom any correspondence should be addressed.

E-mail: hkomatsu@coh.org

Keywords: spheroid culture, micropatterned dish, pancreatic islets, 3D spheroid, high seeding density culture

Supplementary material for this article is available [online](#)

Abstract

The need for maintaining cell-spheroid viability and function within high-density cultures is unmet for various clinical and experimental applications, including cell therapies. One immediate application is for transplantation of pancreatic islets, a clinically recognized treatment option to cure type 1 diabetes; islets are isolated from a donor for subsequent culture prior to transplantation. However, high seeding conditions cause unsolicited fusion of multiple spheroids, thereby limiting oxygen diffusion to induce hypoxic cell death. Here we introduce a culture dish incorporating a micropyramid-patterned surface to prevent the unsolicited fusion and oxygen-permeable bottom for optimal oxygen environment. A 400 μm -thick, oxygen-permeable polydimethylsiloxane sheet topped with micropyramid pattern of 400 μm -base and 200 μm -height was fabricated to apply to the 24-well plate format. The micropyramid pattern separated the individual pancreatic islets to prevent the fusion of multiple islets. This platform supported the high oxygen demand of islets at high seeding density at 260 islet equivalents cm^{-2} , a 2–3-fold higher seeding density compared to the conventional islet culture used in a preparation for the clinical islet transplantations, demonstrating improved islet morphology, metabolism and function in a 4 d-culture. Transplantation of these islets into immunodeficient diabetic mice exhibited significantly improved engraftment to achieve euglycemia compared to islets cultured in the conventional culture wells. Collectively, this simple design modification allows for high-density cultures of three-dimensional cell spheroids to improve the viability and function for an array of investigational and clinical replacement tissues.

1. Introduction

Three-dimensional (3D) cell spheroids are advantageous over two-dimensional (2D) cultured cells in mimicking the complex microenvironment of living organisms with their active cell-cell interaction and spatial communication [1–3]. Cultures of 3D spheroids are critically important for disease

modeling and drug screening applications to reproduce the physiological environment *in vitro* [4–8]. Other applications include the maintenance of 3D functional spheroids for cell therapies, which are transplanted for the supplementation of lost tissue/organ functions of the human body [9, 10]. In light of the recent rapid progress of stem cell biology, cell therapy applications are expanding [11], and

thus the need for cultures of 3D spheroids is increasing. However, maintaining 3D spheroids in culture is challenging and requires more technical innovation than the 2D culture to effectively supply sufficient oxygen (O_2) and nutrients for their survival while limiting the loss of native 3D architecture and facilitating simple operability.

Cultured cells receive essential molecules such as oxygen and nutrients and eliminate metabolic byproducts through passive diffusion within the culture media; this is in contrast to the convective transport of molecules via fine microvessel networks proximal to cells in living tissue, which provides an optimal microenvironment. The limitation of molecular diffusion within 3D spheroids is lethal for cell survival; especially the depletion of O_2 induces central necrosis, and therefore cell viability of cultured 3D spheroids is inversely correlated to size [12–14].

Three dimensional spheroids are not only generated and grown from single cells but can be isolated from native organs. For example, pancreatic islets are the spherical units in the pancreas that typically are 100–500 μm in diameter [15]. Since islets play a critical role in glucose homeostasis as an endocrine micro-organ, isolated islets have been used for the allo- and auto-transplantation to treat a certain type of diabetes when the native islet function is totally impaired [9, 16–19]. Typically, $\sim 500\,000$ islet spheroids (islet equivalent (IEQ) [15]) are isolated from an organ donor to transplant within several days. While waiting for recipients to be ready for the transplantation, culturing 3D spheroid islets is a critical step; in fact, both the quality and quantity of the islets rapidly decrease during the conventional cultures in just a few days, limiting clinical application efficacy.

In the current clinical setting, culturing islets is performed as static incubation in polystyrene flasks that limit the O_2 supply. The flask is also flat-bottomed, and islet distribution in the flask is not well controlled, further exacerbating the diffusion imbalance within the culture media. These issues limit the islet seeding density; thus, islets are cultured at ~ 100 IEQ cm^{-2} , which requires many flasks to accommodate isolated islets from a donor prior to the transplantation. Handling many flasks, i.e. seeding maintenance, and collection of islets in an aseptic procedure before transplantation, is a strenuous task with the risk of contamination, which is behind the scenes of islet delivery to patients.

Several methods have been explored to address the limited diffusion of the essential molecules in 3D spheroid culture. Exogenous oxygenation was applied to reduce central necrosis and improve the viability of statically cultured pancreatic islets [13, 20–23]. Further, perfusion chambers provide convective transport to mimic physiological tissue fluid movement,

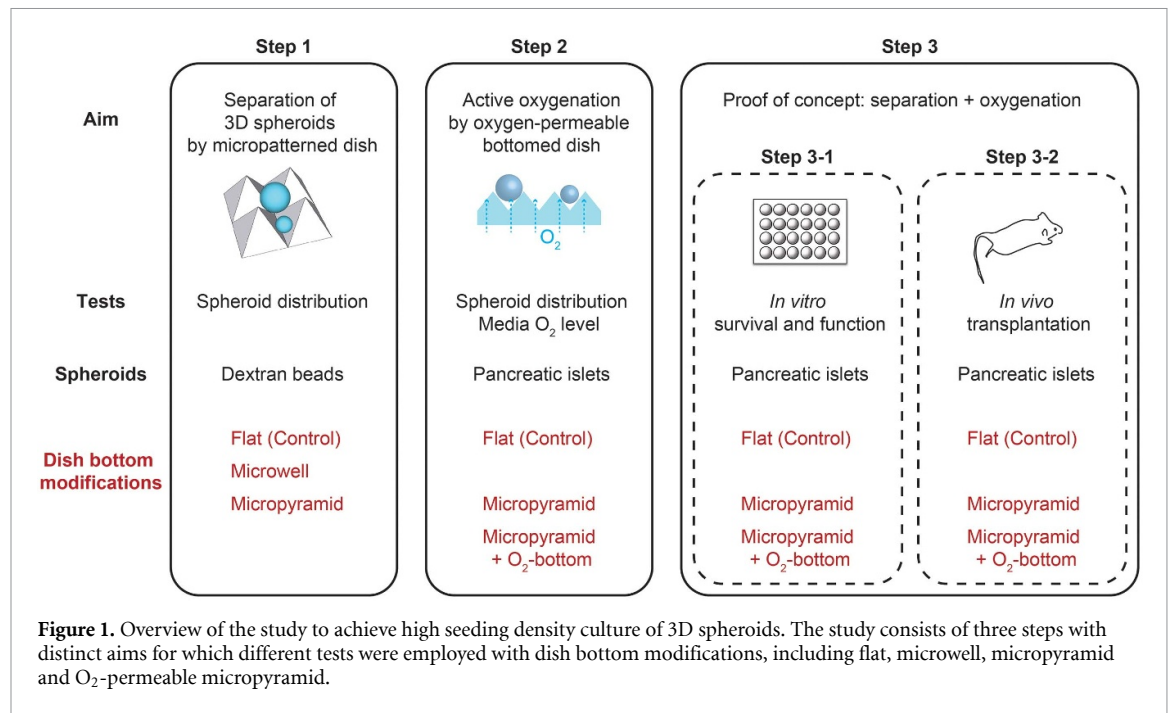
which reduces the gradient of the essential molecules [24–26]. Although these approaches are promising, culturing at high seeding density is still challenging. Controlling the spheroid distribution within a culture flask is especially important; otherwise, spheroids fuse to generate huge constructs. In fact, the above-mentioned approaches do not improve the limited intra-spheroid diffusion within the large spheroids.

In this study, we engineered a micropyr- amid-patterned, oxygen-permeable bottomed dish to achieve a 2–3-fold increase in cell seeding density while preserving the quality and function of the islet cells, reducing laborious preparatory workload and contamination risks. Our culture dish draws additional oxygen transport paths not only from the bottom of the culture dish but also by generating interstices between the islets. Relevant to the clinical islet transplantation preparation period for 3–4 d, we tested the short-term effect of the micropyr- amid-patterned, oxygen-permeable bottomed dish in comparison to the conventional flat-bottomed dish on the biological outcomes, including *in vitro* viability, metabolism and function followed by the *in vivo* function assessment of cultured islets (figure 1).

2. Method

2.1. Fabrication of micropyr- amid-patterned culture dishes

Culture dishes were prepared with three different types of bottom surfaces in a 24-well format with an area of 1.9 cm^2 in each well. These types were: (a) a conventional flat surface (SARSTEDT, Newton, NC, USA), (b) a microwell array (Aggrewell 400, STEMCELL Technologies, Vancouver, Canada), and (c) a micropyr- amid-patterned array. The micropyr- amid structure was designed to have the inverse topography of Aggrewell 400 plates' microwell array. Polydimethylsiloxane (PDMS; Dow Sylgard 184, 1:10 mixing ratio, Ellsworth Adhesives, Germantown, WI, USA) was poured into a dish of six-well Aggrewell 400 plate (mold) to fabricate micropyr- amid arrays, then incubated at 25 $^\circ\text{C}$ for 48 h on a leveled surface to cure the micropyr- amid-patterned PDMS sheets. Each micropyr- amid-patterned PDMS was peeled from a mold and cut using a hollow punch for the subsequent process (figure 2(A)). To fabricate the micropyr- amid-patterned PDMS sheets of different thicknesses, 0.4, 0.5, 0.6 or 1.0 ml of PDMS were poured into the six-well Aggrewell 400 plate to fabricate molded PDMS sheets of 150, 250, 400, and 800 μm in thickness, respectively (figures 2(B) and (C)). PDMS thickness was measured in cross-sectional images through the middle of the sheet (microscopy: SZ61, Olympus; Infinity2, Teledyne Lumenera; image processing: cellSens, version 1.12, Olympus). The PDMS sheet thickness was defined as the distance



from the culture dish bottom surface to the base of the micropyramids.

Non-O₂-permeable, micropyramid-patterned bottom culture plates were fabricated by punching out a circle 12.3 mm in diameter from an 800 μm -thick micropyramid-patterned PDMS sheet to match the inner diameter of dishes in 24-well plates. To fabricate O₂-permeable, micropyramid-patterned bottom culture plates, a round micropyramid-patterned PDMS sheet 15.9 mm in diameter (i.e. 3.6 mm larger than the inner diameter of a 24-well) was prepared and glued to the bottom of a 24-well no-bottom plate (Greiner Bio-One, Monroe, NC, USA) using a medical-grade epoxy (MasterSil 912Med, Master Bond, Hackensack, NJ, USA). The glue was applied exclusively to the region of overlap. After curing the epoxy, 1 ml of distilled water was poured into the dishes and left for 24 h at room temperature to confirm the absence of leakage at the sealed interface. Figure 2(D) illustrates the schematic cross-section of the fabricated wells.

2.2. Seeding test of microsphere beads

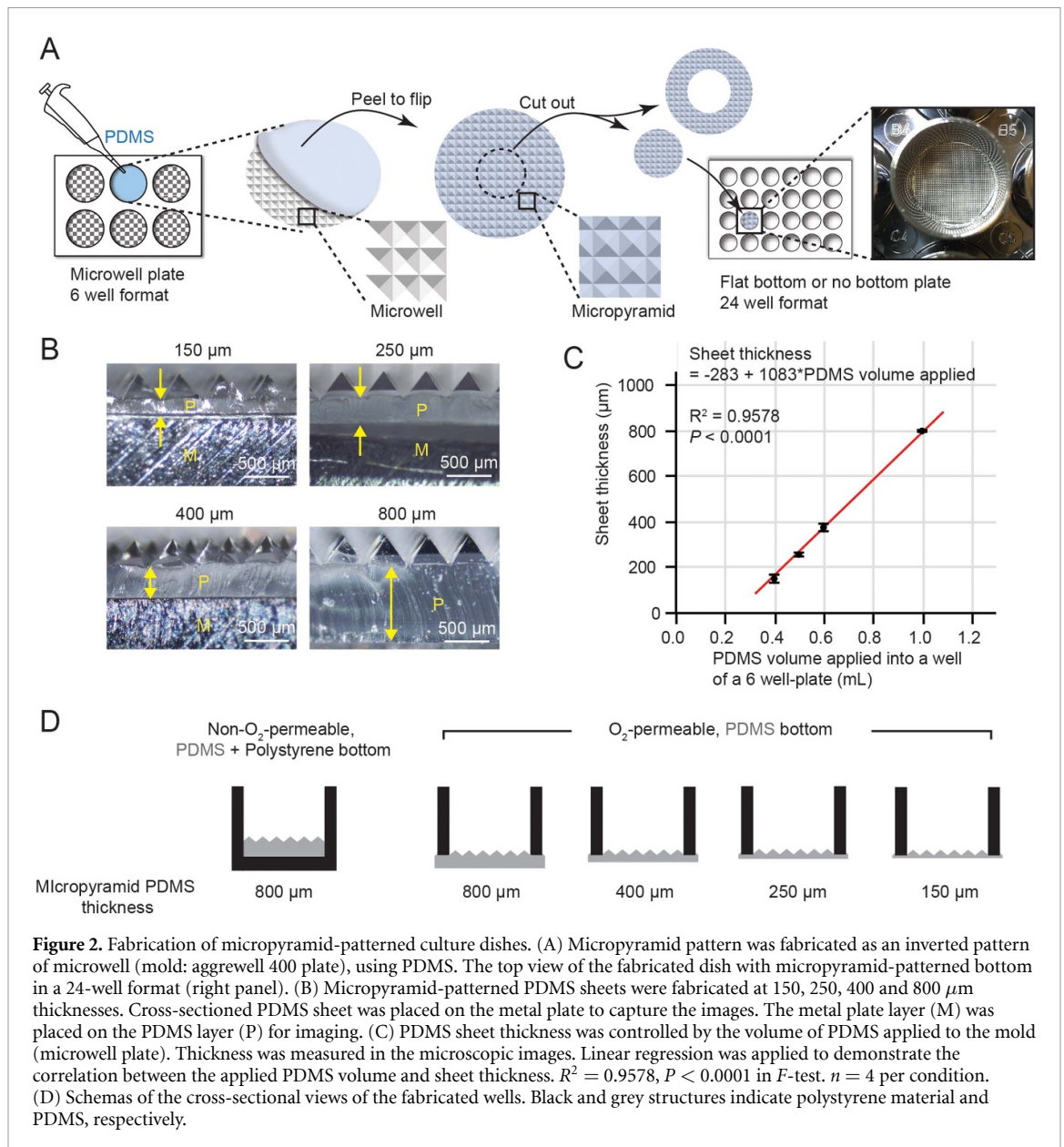
Spherical dextran beads were used to test the distribution of 3D spheres on the culture dishes (Cytodex 1, Sigma-Aldrich St. Louis, MO, USA). Beads were swelled to $\sim 190 \mu\text{m}$ (range: 150–300 μm) in diameter by incubation in distilled water overnight at 4 °C. Beads were then colored in a Methylene Blue solution (Sigma-Aldrich) overnight at 4 °C for visualization, followed by the washing steps in distilled water.

Colored dextran beads were seeded into a 24-well culture plate with 1 ml of phosphate-buffered saline (PBS; Corning Life Sciences, New York, USA),

with three different bottom structures: flat, microwell and micropyramid. Two seeding-density conditions at 200 and 400 beads per dish were tested. Beads were applied to the dishes, mixed with pipetting, and left undisturbed for 10 min for the beads to sediment, then imaged using the bright field (microscope: SZ61, Olympus; camera: Infinity2, Teledyne Lumenera, Ottawa, ON, Canada). The beads distribution was categorized into single, two-bead-aggregate, and \geq three-bead-aggregate, and the number of beads in each category was counted. Four individual experiments were performed for each condition.

2.3. Preparations of pancreatic islets and culture

Islets were isolated from wild-type Lewis (LEW) rats for all studies except the islet metabolism examinations, in which Luciferase-transgenic (Luc-Tg) LEW rats were used as donors for bioluminescent imaging [27]. Islets were isolated using the following procedures [28, 29]. Under general anesthesia, 9 ml of ice-cold collagenase solution (2.5 mg ml⁻¹ in Hanks' Balanced Salt Solution (HBSS), Sigma-Aldrich) was injected into the pancreatic duct through the common bile duct. The distended pancreas was resected and enzymatically digested at 37 °C for 10 min. The digested pancreas was centrifuged at 300 $\times g$ for 3 min. Pellets were subjected to density gradient centrifugation in HBSS solution and Histopaque-1077 (density: 1.077 g ml⁻¹, Sigma-Aldrich) for 25 min at 300 $\times g$. Islets were hand-picked for purity. Since isolated islets are heterogeneous in size, the standardized unit of IEQ was used to count the volume-based, normalized islet number, in which the islet with 150 μm in diameter is defined as 1 IEQ [15].



Prior to the subsequent *in vitro* culture tests, islets were recovered from the isolation process by the overnight incubation at 27 °C at low seeding density (11–15 IEQ cm^{-2} , in a 95 mm-petri dish [Corning Life Sciences) using 8 ml of CMRL 1066 culture media (Corning Life Sciences) supplemented with 0.5% human serum albumin, 0.1 $\mu\text{g ml}^{-1}$ insulin-like growth factor-1 (Cell Sciences, Newburyport MA, USA), 10 U ml^{-1} heparin sodium (Sagent Pharmaceuticals, Schaumburg, IL, USA), and Penicillin-Streptomycin-Glutamine (Gibco, Waltham, MA, USA) in a 5% CO_2 -incubator at 27 °C. Recovered islets, defined as ‘pre-cultured islets,’ were retrieved, counted, and seeded into the designated conditions of subsequent culture at 37 °C with freshly prepared culture media. All islet culture experiments were performed in a 24-well format at high seeding density (260 IEQ cm^{-2} (500 IEQ/dish)) with 1 ml of culture

media, except the first preliminary experiment at 100 IEQ cm^{-2} which is similar islet density condition used in the clinical islet transplantation preparations (86–114 IEQ cm^{-2} (15 000–20 000 IEQ/T175 flask)).

2.4. Seeding/movement test of isolated islets

Two culture dishes were prepared to assess the movement of islets during culture: conventional flat-bottom and micropyramid-patterned bottom. Two hundred IEQ per dish of isolated islets were seeded with gentle pipetting and left undisturbed for 10 min to sediment. The distribution of islets was imaged in the bright field (SZ61, Olympus; Infinity2, Teledyne Lumenera) on days 0 and 3. To analyze the movement (migration) of islets, the bottom area of the 24-well plate was categorized into 4 concentric zones on the captured images (zone 1 for the center and

zone 4 for the periphery); each zone had the same area of 0.478 cm². The islet number in each zone was counted on day 0 and day 3. The percent increase of the islet was defined as migration index.

Migration index (%)

$$= \frac{(\text{islet number on day 3}) - (\text{islet number on day 0})}{(\text{islet number on day 0})} \cdot 100.$$

For example, when the islet numbers are the same between day 0 and day 3 in a specific zone, migration index = 0%. Three individual experiments were employed in each condition.

2.5. Culture media flow simulation

The culture media generates media dynamics as the temperature changes after the culture dish is placed in the 37 °C incubators. The media flow simulation in a 24-well plate was employed using a finite volume method in SOLIDWORKS Flow Simulation (Service Pack 5.0, 2019, SOLIDWORKS Waltham, MA, USA). Navier–Stokes equations were applied to govern the fluid dynamics simulation. The simulation structure is based on the 24-well plate geometry placed on the heated incubator shelf with four different layers from bottom to top: (a) aluminum shelf layer at 37 °C, (b) polystyrene layer at 22 °C, (c) water (instead of culture media) layer at 22 °C, and (d) air layer at 37 °C. Cultured islets on the bottom of the dish were not involved in the flow simulation. Simulation data 10 s after placing the 24-well plate in the incubator was obtained.

2.6. Simulation of pO₂ distribution

A finite element method (COMSOL Multiphysics 5.3, Stockholm, Sweden) was used to examine the O₂ gradient formed in the microenvironment of the culture media in a 24-well plate. The O₂ transport properties were characterized using Fick's diffusion equation with the consumption term:

$$\frac{\partial c}{\partial t} = D\nabla^2 c - R \left[\frac{\text{mol}}{\text{m}^3 \cdot \text{s}} \right]$$

where c is the O₂ concentration, D is the diffusion constant of O₂, and R is the O₂ consumption rate of cells governed by the Michaelis-Menten type metabolic kinetics:

$$R = \text{OCR} \left(\frac{c}{c + K_m} \right) \left[\frac{\text{mol}}{\text{m}^3 \cdot \text{s}} \right]$$

where OCR denotes the maximum O₂ consumption rate achievable by the islets and K_m represents the O₂ concentration at which the rate equals to half of the maximum. Henry's law was also used to correlate the O₂ concentration with O₂ tension so the continuity of O₂ partial pressure can be applied across different boundaries:

$$c \left[\frac{\text{mol}}{\text{m}^3} \right] = H \left[\frac{\text{s}^2 \text{mol}}{\text{kg m}^2} \right] \cdot p\text{O}_2 [\text{Pa}]$$

where H is the O₂ solubility and $p\text{O}_2$ is the partial pressure of oxygen.

The simulation geometry (figure S1(A)) is based on the 24-well plate geometry with three different layers from bottom to top: (a) the bottom layer, consisting of either oxygen impermeable polyester or oxygen-permeable PDMS membranes with different thicknesses, (b) active O₂ consumption layer, which consists of islets and culture media, and (c) top culture media layer. In the active O₂ consumption layer, four different concentric zones with the same footprint size were constructed by homogenizing the O₂ consumption rate and the corresponding parameters based on the measured islet density (figure S1(B)). A complete list of parameters used for the simulation of pO₂ is in supplemental table 1.

2.7. pO₂ measurements of culture media

The O₂ microenvironment in the post-culture media was examined *in vitro* after the 3 d-culture using 300 and 600 IEQ per well. An optic, flexible wire-type O₂ probe to measure the pO₂ in the media (Ocean Optics, Dunedin, FL, USA) was placed on a rotary positioner (Parker Hannifin, Irwin, PA, USA) for fine spatial positioning, and the tip of the probe was placed in the designated points. pO₂ measurements were employed to examine the two types of O₂ gradient in the culture media, namely, transverse O₂ gradient and vertical O₂ gradient.

Transverse O₂ gradient was assessed by the difference of pO₂ ($\Delta p\text{O}_2$) between two points in the bottom layer of the well. pO₂ were measured at the center of the well (pO_{2_ctr}) and 0.4 cm away from the center (pO_{2_perif}), and transverse $\Delta p\text{O}_2$ ($\Delta p\text{O}_2_{\text{trans}}$) was defined as $\Delta p\text{O}_2_{\text{trans}} = p\text{O}_2_{\text{perif}} - p\text{O}_2_{\text{ctr}}$. Transverse O₂ gradient was examined in two culture conditions with a flat bottom or micropyramid-bottom dish, and three individual experiments were employed for reproducibility.

Vertical O₂ gradient was assessed by the difference of $\Delta p\text{O}_2$ between two points in the center of the well. pO₂ was measured at the bottom of the well (pO_{2_btm}) and 0.4 cm upper from the bottom (pO_{2_upr}), and vertical $\Delta p\text{O}_2$ ($\Delta p\text{O}_2_{\text{vert}}$) was defined as $\Delta p\text{O}_2_{\text{vert}} = p\text{O}_2_{\text{upr}} - p\text{O}_2_{\text{btm}}$. Vertical O₂ gradient was examined in the five micropyramid-patterned bottom conditions, including a non-O₂-permeable bottom and O₂-permeable PDMS bottoms (150, 250, 400, and 800 μm in thickness). Three individual experiments were performed in each condition.

2.8. Oxygen consumption rate of the isolated islets

The OCR of the isolated rat islets was measured for the pO₂ simulations. Isolated islets were recovered from the isolation process by the overnight incubation at 27 °C at low seeding density as described in *Preparations of pancreatic islets and culture*, followed by the pre-incubation at 37 °C for 4 h prior to

the OCR measurement in a 95 mm-petri dish. Islet OCR was measured using a Seahorse XFe analyzer (Seahorse Bioscience, North Billerica, MA, USA). Approximately 100 IEQ per donor were plated onto wells in a Seahorse XFe islet capture plate with the RPMI media containing 3 mM glucose. Seven islet OCR measurements were employed every 7.5 min to calculate the average OCR. The exact islet number applied was calculated by the image analysis for the conversion to IEQ (cellSens, Olympus). Data were obtained from five different donors.

2.9. Islet morphology and viability assessment

Bright-field images of cultured islets were captured to assess the islet morphology (SZ61, Olympus; Infinity2, Teledyne Lumenera). Shape factor, which numerically describes the shape of a particle in 2D images [30], was calculated for the cultured islets:

$$\text{Shape factor} = 4 \cdot \pi \cdot \left(\frac{\text{area}}{\text{perimeter}^2} \right)$$

where the *area* and *perimeter* of individual islets were measured. Shape factor values can range from 0 to 1, where the value of 1.0 indicates a perfect spheroid. Fifty cultured islets were incubated in 0.48 μM of fluorescein diacetate (FDA; Sigma-Aldrich, Saint Louis, MO, USA) solution in PBS for 5 min in the dark at room temperature, washed with PBS, and gently transferred to a 96-well plate to capture the fluorescent images (IX50, Olympus) to calculate the shape factor (cellSens, Olympus).

Islet mass was assessed by calculating the islet area using bright-field photomicrographs (IX50, Olympus) [22, 31]. Briefly, 2D islet area was analyzed by cellSens imaging software (Olympus), followed by the conversion to the unit of IEQ (1 IEQ represents the islet 150 μm in diameter; 17 671 $\mu\text{m}^2/\text{IEQ}$ in 2D area analysis) [15]. Islet mass was evaluated on day 0 (pre-culture) as well as day 4 (post-culture).

Islet viability was analyzed using live/dead staining by a semi-automated method [22, 32]. Cultured islets (100 IEQ per group) were incubated in 0.48 μM and 15 μM of FDA/propidium iodide (PI; Sigma-Aldrich) solution in PBS for 5 min in the dark at room temperature, washed with PBS, and gently transferred to a 96-well plate to capture the fluorescent images (IX50, Olympus). Overall viability of all islets imaged was calculated using the cellSens software (Olympus) as previously described [32].

The occurrence of islet fusion was evaluated using the live/dead staining images. Fusion was defined by the structure of 2 or more islets tightly attached, and islets were categorized as 'Single' or 'Fused.' Especially for the viability assessment of Single vs. Fused, the viability of individual constructs ($n = 45$ for Single and $n = 35$ for Fused) was calculated. The 2D area of the islet constructs (including Single and Fused) was also measured using the same images to analyze the islet size.

2.10. Islet damage assessments

Cell damage of post-cultured islets was assessed using the 3 day-cultured islets. HMGB1 is the ubiquitous nuclear protein, and secreted HMGB1 has been used as a biomarker of non-cell-type-specific damage by necrotic cells to trigger inflammation [33–35]. HMGB1 released into the culture media was measured using an HMGB1 Detection Kit (Chondrex, Woodinville, WA, USA), and HMGB1 concentration was normalized by IEQ seeded on day 0.

Insulin content in the post-cultured islets was examined for beta cell-specific damage. Approximately 100 IEQ of islets were sampled and lysed in 1 ml of cell lysate buffer composed of 70% ethanol (v/v; Sigma Aldrich) and 0.09 mol l^{-1} of Hydrochloric acid (as final concentration; Sigma Aldrich) dissolved in distilled water [36]. The insulin concentration of the islet lysate was measured using a rat insulin ELISA kit (Merckodia, Uppsala, Sweden). Before islets were lysed, accurate islet mass (in the unit of IEQ) was measured by image analysis (cellSens, Olympus, Tokyo, Japan), with which insulin content data was normalized. Three independent experiments were performed for HMGB1 and insulin content measurements.

2.11. Histological examinations of cultured islets

In vitro cultured islets were fixed in 10% formalin and embedded in 3% agar for histological sectioning. H&E stain was performed for morphological assessment. For the detection of cellular hypoxia, immunohistochemistry (IHC) was performed on Ventana Discovery Ultra IHC autostainer (Roche Diagnostics, Indianapolis, IN, USA) using HIF1A primary antibody (MA1-16 504, Thermo Fisher Scientific, Waltham, MA, USA; dilution at 1:100) and Discovery HQ-HRP-DAB detection system (DISCOVERY anti-Mouse HQ and DISCOVERY anti-HQ HRP). Images were captured using an IX50 microscope (Olympus) and cellSens software (Olympus). For the islet damage assessment, the pyknotic area, characterized by nucleus deformation and loss of cytoplasm with an eosin-negative area, was detected and measured in the image analysis (cellSens, Olympus), to calculate the % pyknotic area to the whole islet area [37]. The overall % pyknotic area/islet area of 10–20 islets were assessed from a single islet preparation, and the data from three individual experiments were presented.

2.12. Gene expression assays (qPCR)

RNA was isolated from 200 IEQ of islets 3 d after *in vitro* culture (TRI Reagent, Molecular Research Center, Cincinnati, OH, USA, and Direct-zol RNA Microprep, Zymo Research, Irvine, CA, USA) for following real-time PCR, as described previously [38]. Relative quantities of each transcript (hypoxia-related genes (HIF1-target genes)) were normalized to an endogenous housekeeping gene (*ACTB*) and

expressed as a fold-increase to the average of CTL. All primers for *VEGFA* (Rn01511602_m1), *GAPDH* (Rn01775763_g1), *SLC2A1* (Rn01417099_m1), and *ACTB* (Rn00667869_m1) were obtained from Thermo Fisher Scientific (Waltham, MA, USA). Gene expression data were obtained from three independent experiments.

2.13. Islet metabolism

In vitro islet metabolism of isolated islets from LUC transgenic rats [27] was assessed using an ATP-based bioluminescent intensity assay [39]. Three-day cultured islets at 500 IEQ/well in a 24-well plate were incubated in luciferin solution (PerkinElmer, Waltham, MA; 150 $\mu\text{g ml}^{-1}$ dissolved in the culture medium) for 20 min at 37 °C. Then bioluminescent images were captured over 60 s per image (Lago X platform, Spectral Instruments Imaging, Tucson, AZ, USA). Images of three independent experiments were obtained, and bioluminescent intensities were normalized by the IEQ number applied.

2.14. Islet function

Glucose stimulated insulin secretion (GSIS) was assessed using post-cultured islets on day 3 after high seeding density culture. Approximately 200 IEQ per well were incubated on a 24-well plate cell culture insert (Millipore Sigma, Burlington, MA, USA) with 1 ml of Krebs–Ringer buffer (KRB) solution containing 2.8 mM glucose for 1 h, followed by a 1 h incubation with 1 ml of KRB solution containing 28 mM glucose. After each incubation, the buffer was collected to measure insulin concentration using a rat insulin ELISA kit (Merckodia). After the high glucose incubation, islets were lysed in the well using 1 ml of cell lysate buffer. The insulin concentration of the samples was measured using a rat insulin ELISA kit (Merckodia, Uppsala, Sweden). Data of secreted insulin in low and high-glucose KRB solutions were normalized using total insulin content in islets [36, 39]. The insulin secretion ratio between high glucose over low glucose was used to calculate the stimulation index (SI_GSIS). Three independent experiments were performed.

2.15. *In vivo* transplantation of cultured islets

Streptozotocin (STZ)-induced diabetic NOD-SCID mice (Charles River Laboratories, Wilmington, MA, USA) were used as recipients for islet transplantations under the renal capsule of left kidneys, as previously described [40, 41]. Mice were injected intraperitoneally with STZ (50 mg kg^{-1} -body weight of mouse) for 3 consecutive days for 2 weeks before the transplantations to induce diabetes. Before the islet transplantation, diabetes was confirmed by measuring blood glucose levels at $>400 \text{ mg dl}^{-1}$.

Four-day-cultured islets were handpicked to prepare the designated IEQ required for the study under the microscope (SZ61, Olympus). Digital images of

handpicked islets were obtained (Infinity2, Teledyne Lumenera) to measure and confirm the IEQ in cellSens software (Olympus). In the initial study, pre-cultured islets were transplanted to examine the marginal islet number to reverse diabetes in this animal model: 100 IEQ ($n = 3$), 200 IEQ ($n = 3$), 300 IEQ islets ($n = 1$) and 400 IEQ ($n = 1$). In subsequent *in vivo* experiments, 200 IEQ of 4 day-cultured islets in three different culture conditions (flat-bottom (CTL), microwell, and micropyramid bottom) were transplanted ($n = 4$ per condition).

Non-fasting blood glucose levels were measured weekly for 7 weeks after the transplantation, and reversal of diabetes was defined as blood glucose below 200 mg dl^{-1} for two consecutive weeks. Area under the curve (AUC) of the blood glucose in the observation period between 0 and 6 weeks (AUC_0–6 weeks) was calculated and expressed in the unit of $\text{mg/dL} \cdot \text{week}$ to quantify the post-transplant glycemic control [42, 43]. For the mice in which diabetes was reversed, kidneys with transplanted grafts were resected to confirm the increase of blood glucose without functional islet grafts.

As an *in vivo* functional assessment of transplanted islets, an intraperitoneal glucose tolerance test (IPGTT) was employed 4 weeks after the transplantations. Recipient mice fasted for 6 h before an intraperitoneal administration of glucose solution at 2 g glucose kg^{-1} body weight to assess glucose tolerance [44]. Blood glucose was measured at 0, 15, 30, 60 and 120 min after the glucose injection. AUC of the blood glucose between 0 and 120 min (AUC_0–120 min) was calculated and expressed in the unit of $\text{mg/dL} \cdot \text{min}$ [39] to quantify the IPGTT data.

The long-term systemic effect of islet transplantation was also evaluated by the occurrence of diabetic nephropathy, a representative complication of diabetes mellitus [45–47]. At the end of the study at 6–7 weeks, kidneys were resected to fix in 10% formalin for histology sectioning. Periodic acid-Schiff (PAS) staining with the hematoxylin counterstain was performed for the assessment of the mucopolysaccharides deposition in the glomerulus (Periodic Acid-Schiff Kit, Sigma Aldrich). The average % PAS-positive area/glomerulus area was quantified from ten glomeruli in each recipient (cellSens, Olympus).

The use of animals and animal procedures in this study were approved by the City of Hope/Beckman Research Institute Institutional Animal Care and Use Committee.

2.16. Statistical analysis

Data were reported as the mean \pm standard error (SEM). Statistical analyzes were performed using the JMP 9 program (SAS Institute, Cary, NC, USA). For the statistical comparisons between the averages of two groups, Student's *t*-tests was used. Correlations were analyzed using fitted regression lines and coefficient of determination (R^2) values, and statistical

significance were calculated using *F*-tests. $p < 0.05$ denotes statistical significance.

3. Results

3.1. Reduced viability by the fusion of pancreatic islets during culture

The diffusion of essential molecules into the core of spheroids is suboptimal in large 3D spheroids, inducing cell death [13, 14]. Fused islets act as a single larger unit which detrimentally affects islet survival in cultures [13]. Notably, such fusion frequently occurs in standard flat culture flasks and dishes. We cultured isolated rat islets in a flat-bottomed dish for 4 d at a conventional islet seeding density of 100 IEQ cm^{-2} , similar to the clinical islet transplantation preparation. We found a frequent occurrence of central necrosis in large, fused islets with live/dead staining (figure 3(A)). Viability plots of overall islets and fused islet constructs revealed that the viability negatively correlates to the islet area analyzed in the 2D images (figure 3(B), $\text{viability} = 98.2 - 3.3 \times 10^{-4} \times \text{Islet area}$, $R^2 = 0.25$, $P < 0.0001$). The area of fused islet structures was significantly larger than that of single islets (figure 3(C), $25\,560 \mu\text{m}^2$ vs. $69\,379 \mu\text{m}^2$, $P < 0.0001$). The viability of fused islet structures was significantly lower than that of single islets (figure 3(D), 91.0% vs. 73.6%, $P < 0.0001$). These results indicated that the prevention of islet aggregation could be an important strategy to maintain islet quality during the culture.

3.2. Improved separation of islet-mimicking beads with micropyramid-patterned dish

We examined the distribution of dextran beads on three different surfaces to determine the extent of potential islet separation in culture on these surfaces: (a) flat (conventional culture dish), (b) microwell array, and (c) micropyramid array (figure 4(A)). We hypothesized that the microwell and micropyramid patterns could have a similar effect on spheroid separation in mid-seeding density (figure 4(B)), whereas the micropyramid pattern could be advantageous over microwell, especially at high seeding density (figure 4(C)) since the microwell dish potentially can accommodate multiple spheroids within a well to induce unsolicited aggregation (figure 4(C)). We investigated the actual occurrence of aggregation using beads ranging from 150 to 300 μm in diameter, similar to the size range of the isolated rodent islets used in this study; aggregation was defined as beads in contact in images. At mid-seeding density, an analysis using images of beads in different bottom surfaces (figure 4(D)) revealed that microwell and micropyramid bottoms effectively prevented aggregation as observed for the flat-bottom surface (figure 4(E); 71%, 88%, and 91% of single beads in the flat bottom, microwell, and micropyramid, respectively). Detailed comparison analysis

(figure S2(A)) demonstrated that the occurrence of aggregation is significantly reduced for both microwell and micropyramid patterns when compared to the flat bottom ($P = 0.0001$ (microwell vs. flat bottom) and $P < 0.0001$ (micropyramid vs. flat bottom)). High seeding density increased the occurrence of aggregation in all conditions compared to the mid-seeding density (figures 4(F) and (G)). However, the percentage of single beads was notably highest for the micropyramid array at high seeding density (53, 68, and 80% in the flat bottom, microwell, and micropyramid, respectively), indicating the highest bead separation. Occurrence of aggregation in micropyramid (20%) was significantly lower than that in microwell (32%) (figure S2(B); $P = 0.0422$ (microwell vs. micropyramid)). These results demonstrate the potential use of the micropyramid-patterned bottom for the culture of 3D spheroids, including pancreatic islets, to mitigate islet fusion during the culture.

3.3. Alleviating islet movement-induced O_2 gradient in media by micropyramid-patterned dish

Although the micropyramid-patterned bottom prevented aggregation of beads immediately after seeding, investigators, including ourselves, experimentally know that the seeded islets accumulate in the center of the dish during the culture period, which potentially increases the risk of aggregation via physical islet-islet contact. *In vitro*, we investigated the change in islet distribution between pre-culture (day 0) and post-culture (day 3) in the flat bottom and micropyramid-patterned bottom (figure 5(A)), which demonstrated that islets in the conventional flat bottom showed more movement than those cultured in the micropyramid bottoms. In fact, most of the islets seeded on the micropyramid bottom stayed in the same spot, in the gutter between the micropyrramids (figure 5(A), enlarged pictures), during the culture for 3 d (without culture media replacement). We quantified the change in islet distribution by counting the number of islets in 4 zones in the dish in the captured images (Zone 1 in the center to Zone 4 in the periphery; figure 5(B)). Note that each zone has the same area of 0.478 cm^2 . Analysis revealed that the islets seeded in the flat bottom moved toward the center with the increase of islet population at +165% in Zone 1, -23% in Zone 2, -66% in Zone 3 and -81% in Zone 4, compared to pre-culture. On the other hand, micropyramid showed minimal movement in each zone (5%, -4%, -8%, and +10% in Zone 1-4, respectively). Detailed data are presented in figure S3. Simulation of the culture media dynamics revealed that the temperature increase of the culture media generates the flow from the periphery toward the center in the dish bottom level (figure S4), which could explain the islet movement during culture. These results indicated that the micropyramid-patterned bottom mitigated movement-induced islet aggregation during the culture.

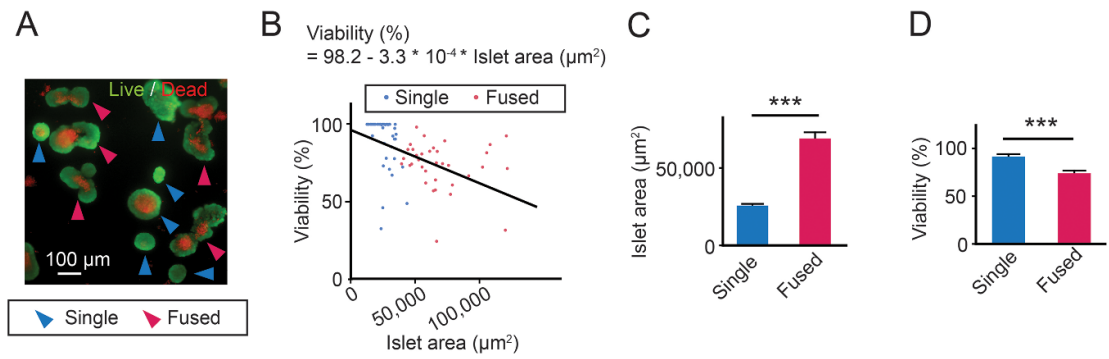


Figure 3. Fusion of pancreatic islets reduces viability *in vitro*. Isolated islets were cultured in a conventional condition at 100 IEQ cm^{-2} on a flat-bottom dish. (A) A representative photo of Live (green)/Dead (red) stain. Single and fused (aggregated) islets were identified. Blue and red arrowheads indicate single and fused islets, respectively. (B) Viability and islet area of single islets ($n = 45$, in blue) and fused islets ($n = 35$, in red) were plotted. Linear regression analysis demonstrated a negative correlation between viability and size of islets. $R^2 = 0.25$, $P < 0.0001$ in F -test. (C) The average area of single and aggregated islets measured in 2D images. $n = 45$ and 35 , respectively. $*** P < 0.001$. (D) Viability of single and aggregated islets measured in 2D images. $n = 45$ and 35 , respectively. $*** P < 0.001$ in Student's t -tests.

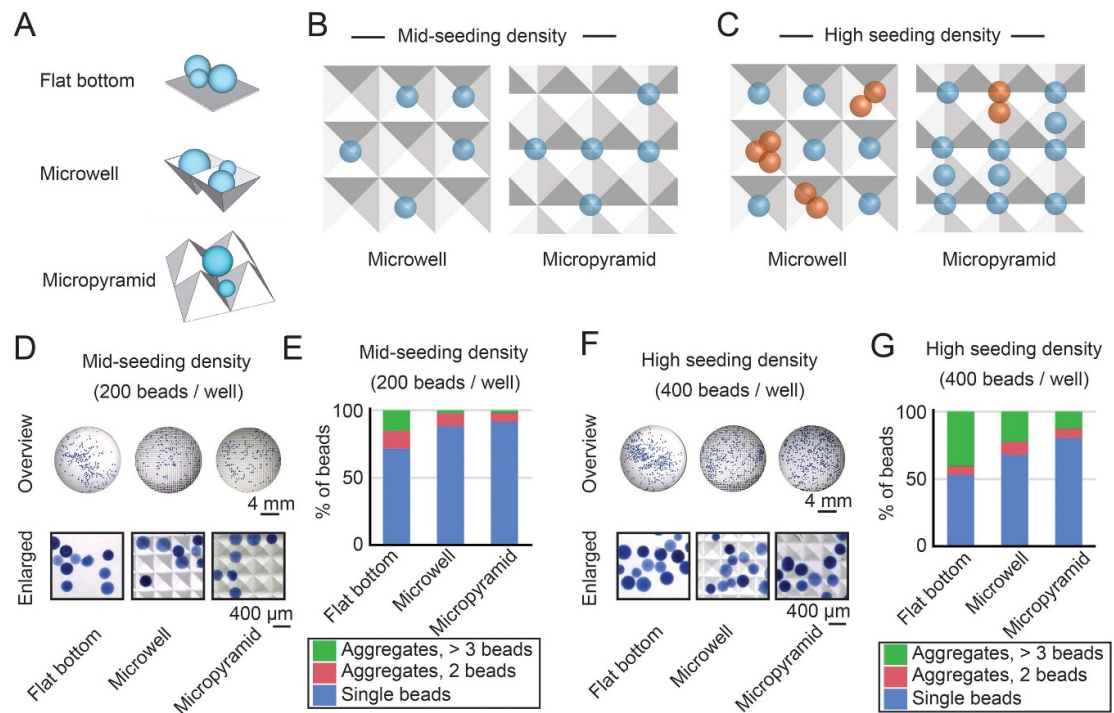
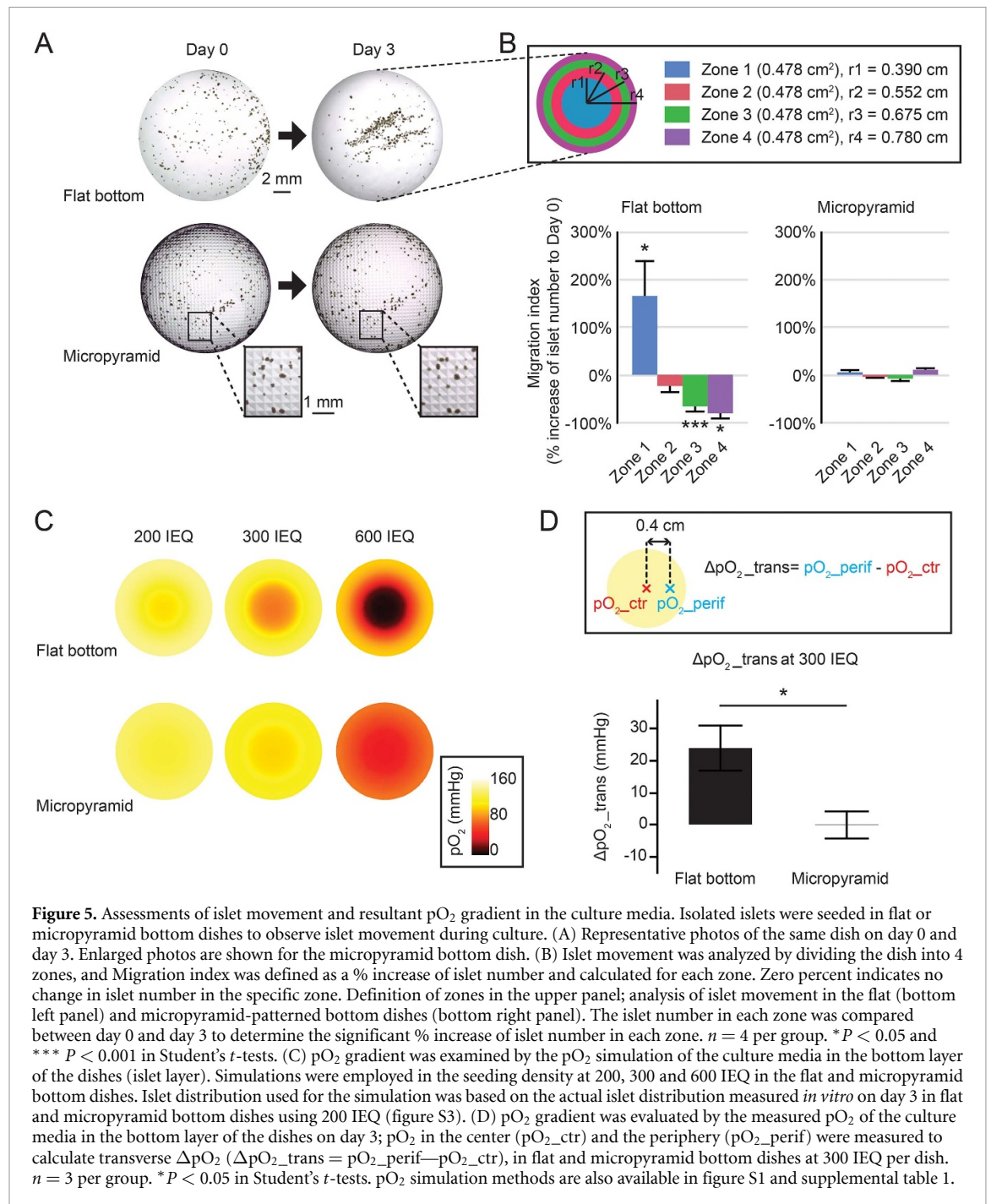


Figure 4. Prevention of aggregation in the culture dish with micropyramid-patterned bottom: islet-mimicking beads model. (A) Schemas of micropatterned bottoms tested: conventional flat, microwell and micropyramid. Blue-colored 3D spheroids are in the micropatterned bottom dishes. (B) Schemas of seeded spheroids in mid-seeding density in microwell and micropyramid patterns. (C) Schemas of seeded spheroids in high seeding density in microwell and micropyramid patterns. Spheroids in contact are colored in orange that can potentially form aggregates in culture. (D) Image of seeded dextran beads (blue; $150\text{--}300 \mu\text{m}$ in diameter) at mid-seeding density in three bottom-patterned dishes in a 24 well-platform. Overview photographs are shown in the upper row and enlarged photographs in the bottom row. (E) Analysis of dextran bead aggregation at mid-seeding density. Seeded beads were categorized into three groups: single, 2 beads and ≥ 3 beads and expressed as % of total beads. Detailed statistical analysis of aggregation is available in figure S3(A). (F) Image of seeded dextran beads (blue; $150\text{--}300 \mu\text{m}$ in diameter) at high seeding density in three bottom-patterned dishes in a 24 well-platform. (G) Analysis of dextran bead aggregation at high seeding density. Detailed statistical analysis of aggregation is available in figure S3(B).

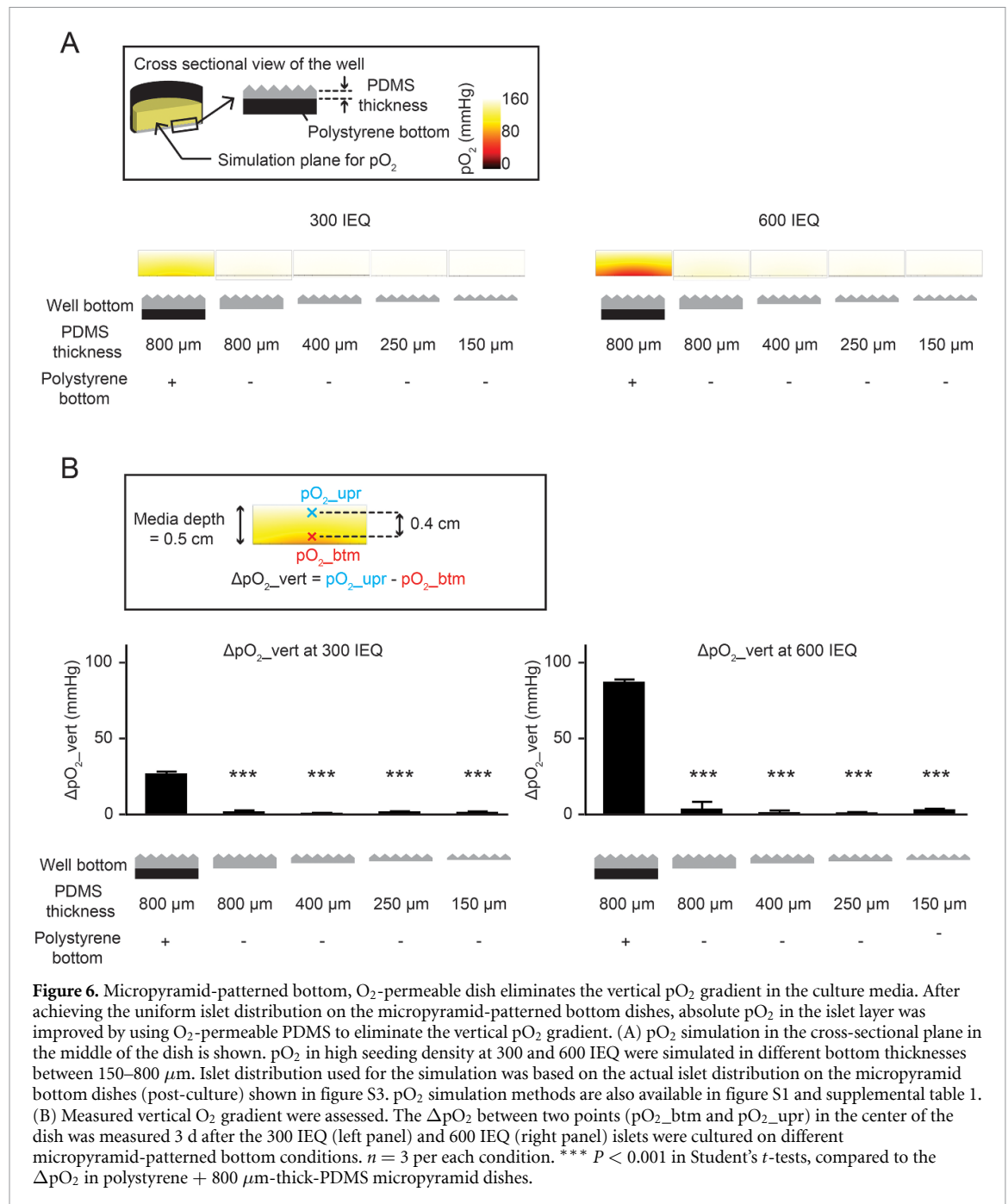
Movement of the islets not only increases the risk of aggregation but also induces the non-uniform islet distribution within the culture dish, which theoretically can create the oxygen tension ($p\text{O}_2$) gradient in the culture media. We simulated the

$p\text{O}_2$ in the bottom layer of the dishes where islets sediment in three conditions at different seeding densities. Note that the islet distribution used for the $p\text{O}_2$ simulation was based on the actual post-cultured islet distribution (figure S3), and the



oxygen consumption rate (OCR) of the islets for the pO₂ simulation was separately measured as $1.84 \text{ pmol sec}^{-1} \text{ IEQ}^{-1}$ (figure S5). As expected, the flat-bottom dishes generated a steeper O₂ gradient compared to the micropyramid bottom dishes in the simulation (figure 5(C)). Further, we measured the pO₂ gradient in the post-culture media with 300 IEQ per dish *in vitro* (figure 5(D)). Micropyramid-patterned bottom dishes diminished the pO₂ gradient, and a more uniform O₂ microenvironment was obtained compared to the flat-bottom dishes ($\Delta pO_2_{trans} = 23.9 \text{ mmHg}$ (CTL) vs. -0.2 mmHg (micropyramid), $P = 0.0429$), which aligned well to

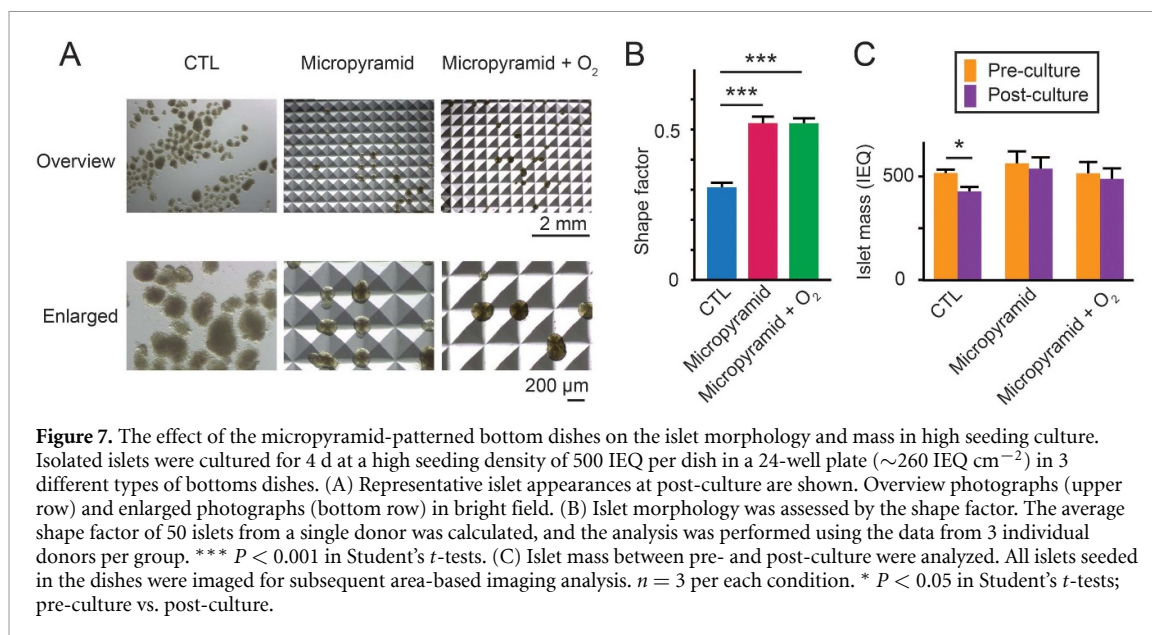
the pO₂ simulation data. These results showed the advantage of the micropyramid-patterned bottom dishes over the flat-bottom dishes in preventing islet movement and creating an O₂ gradient in the culture media. However, pO₂ simulation at higher seeding density (e.g. 600 IEQ) on micropyramid-patterned bottom dishes exhibited an absolute pO₂ level drop in the entire dish area. This result suggested that the external O₂ supply combined with micropyramid-pattern dishes has the potential to improve the O₂ microenvironment, especially in ultra-high seeding density islet cultures, which were tested in the subsequent experiments.



3.4. Eliminating the vertical O₂ gradient by micropyramid-patterned, O₂-permeable bottomed dish

Although the micropyramid-patterned dishes prevented islet fusion and movement, pO₂ on the bottom layer of the dishes dropped, especially in ultra-high seeding density, as shown in figure 5(C), since the micropattern was placed on the O₂-impermeable polystyrene dishes. Therefore, we fabricated the O₂-permeable PDMS-bottomed, micropyramid-patterned dishes in thicknesses between 150 and 800 μm (figure 2). We employed pO₂ simulation in the cross-sectional plane in the middle of the dish (figure 6(A)). Simulations revealed that the

PDMS-bottomed dishes between 150 and 800 μm in thickness effectively improved O₂ environment in the bottom layer of the dishes by minimizing the vertical O₂ gradient at both 300 and 600 IEQ/dish seeding density. To confirm the simulation results, we measured the vertical O₂ gradient *in vitro* culture setting at 300 IEQ and 600 IEQ seeding density (figure 6(B)). The O₂-impermeable polystyrene bottom demonstrated huge vertical O₂ gradient (i.e. pO₂ drop on the bottom compared to the media surface), especially in the high seeding density condition. PDMS-bottomed dishes significantly reduced the vertical O₂ gradient compared to the O₂-impermeable polystyrene bottom in both seeding conditions at 300 IEQ and



600 IEQ ($P < 0.001$). There was no significant difference in vertical O_2 gradients among different PDMS thicknesses tested. These actual measurements were consistent with the simulation data.

Collectively, we demonstrated that (a) micropyramid-patterned bottom dishes alleviated the islet fusion and movement, and (b) additional O_2 -permeability in the bottom layer of dishes further improved O_2 environment of the culture media. Accordingly, in the following experiments, we compared three different types of dish bottoms for islet culture at high seeding density: flat bottom (CTL), micropyramid-patterned bottom (micropyramid), and micropyramidal + O_2 -permeable bottom (micropyramid + O_2). We used a 400 μm -thick PDMS to fabricate the O_2 -permeable bottom dishes due to easier handling than the other PDMS thicknesses and since all thicknesses of PDMS showed similar vertical O_2 gradients.

3.5. Improved islet morphology in high seeding culture on micropyramid-patterned dish

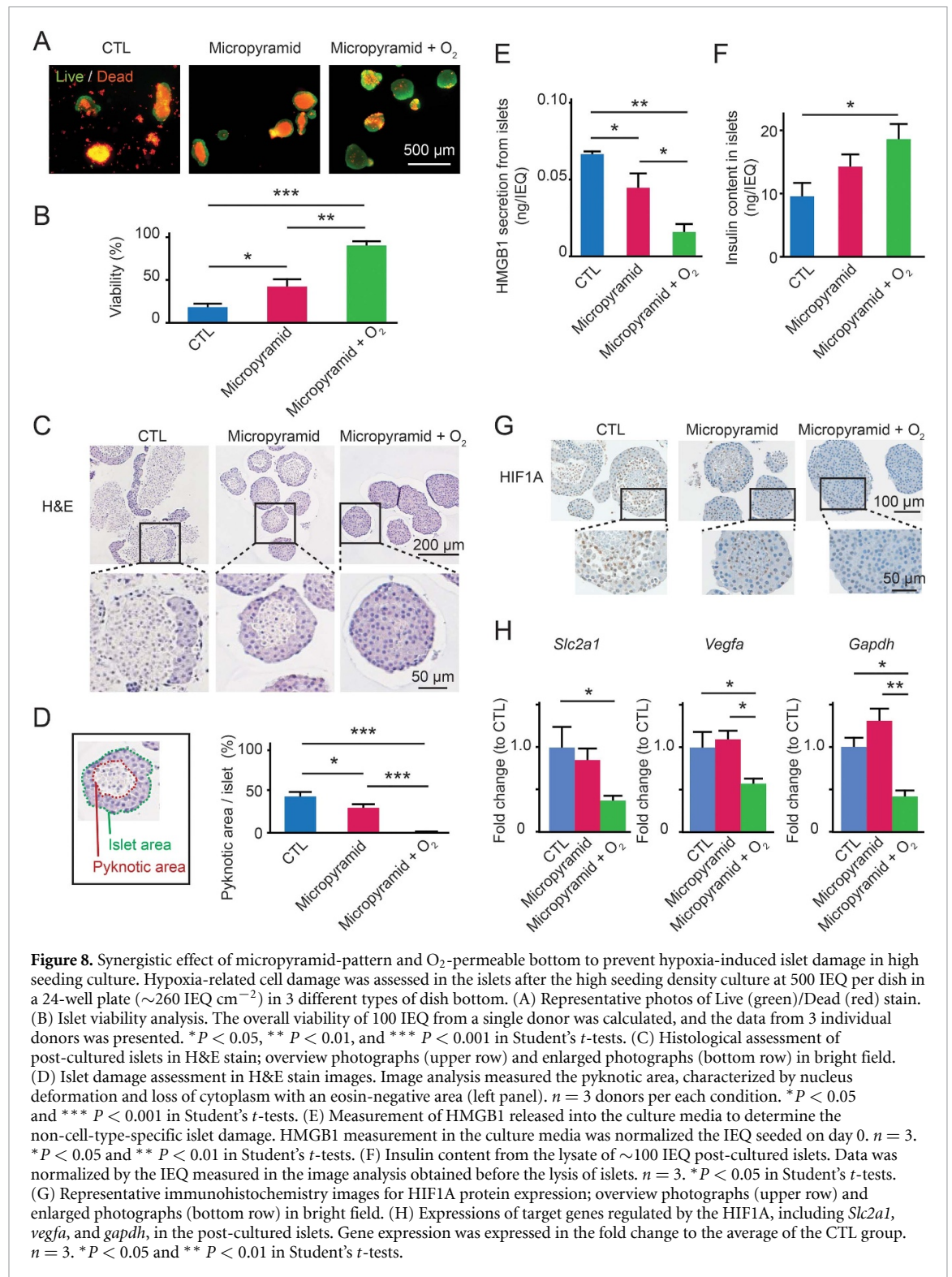
We cultured isolated islets at high seeding density (500 IEQ per dish in a 24-well plate; 260 IEQ cm^{-2}) in three different dish bottoms (CTL, micropyramid, and micropyramid + O_2), shown in figure 7(A). Both micropyramid and micropyramid + O_2 maintained islet morphology well with demarcated borders. In contrast, islets in the CTL dishes had obscure borders, indicating the degraded islets. Further, we evaluated the islet morphology using the shape factor, numerical values describing the shape under 2D images [30]; the micropyramid and micropyramid + O_2 significantly improved the islet morphology compared to the CTL ($P = 0.0002$ (CTL vs. micropyramid) and $P = 0.0002$ (CTL vs. micropyramid + O_2); figure 7(B)). CTL significantly reduced islet mass within 4 d ($P = 0.0312$, pre-culture vs. post-culture),

whereas micropyramid and micropyramid + O_2 alleviated the islet mass reduction (figure 7(C)).

3.6. Mitigation of hypoxia-induced islet damage by micropyramid-patterned O_2 -permeable bottom dish

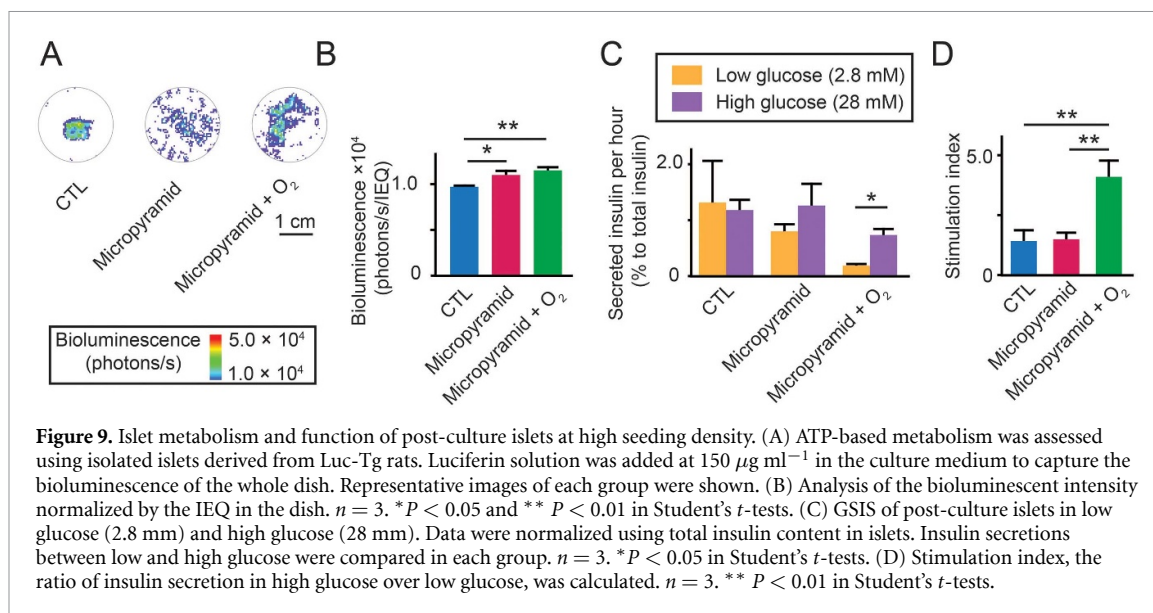
Live/dead stain images of post-cultured islets showed massive islet death with significant debris present in CTL (figure 8(A)). Less debris was present, but islet central necrosis occurred in the micropyramid. In contrast, micropyramid + O_2 minimized islet death. Image analysis demonstrated that the micropyramid-pattern and O_2 -permeable bottoms synergistically improved the islet viability (17.9%, 42.1%, 90.0%, respectively; $P = 0.0309$ (CTL vs. micropyramid), $P = 0.0002$ (CTL vs. micropyramid + O_2); figure 8(B)). Histological examination with Hematoxylin and eosin (H&E stain) showed deformed islets with extensive necrosis and the loss of cytoplasm in CTL (figure 8(C)). Islets cultured in the micropyramid showed round-shaped morphology but with central necrosis characterized by the pyknotic nuclei [37, 48], while micropyramid + O_2 mitigated such cell damage. Image analysis of pyknotic area demonstrated the advantage of the use of micropyramid as well as the O_2 -permeable bottom to alleviate islet damage (figure 8(D)).

We also measured secreted High mobility group box protein 1 (HMGB1) into the culture media, the indicator of the non-cell type-specific islet damage [33–35, 49]. Micropyramid-pattern and O_2 -permeable bottom synergistically reduced HMGB1 released from islets (figure 8(E)). Further, micropyramid + O_2 maintained insulin content significantly better than CTL, indicating the beta cells within the islets were protected from damage (figure 8(F)).



Subsequently, we assessed hypoxia-related islet damage; the IHC showed the accumulation of hypoxia-inducible factor-1 (HIF1A) protein in the nuclei of pyknotic cells, indicating that central necrosis was caused by hypoxia (figure 8(G)). Micropyr amid + O₂ significantly reduced the representative HIF1A target gene expressions, including *Slc2a1*, *Vegfa* and *Gapdh*, when compared to other condi-

tions (figure 8(H)). These data demonstrated that the molecules on the HIF1A pathway were comprehensively altered, further confirming the mitigation of hypoxia in micropyr amid + O₂. Note that *Slc2a1*, *Vegfa* and *Gapdh* are the representative genes regulated by HIF1A [38, 39, 50–52], although *Gapdh* is frequently used as a housekeeping gene.



3.7. Enhanced islet metabolism and function via improved oxygen environment

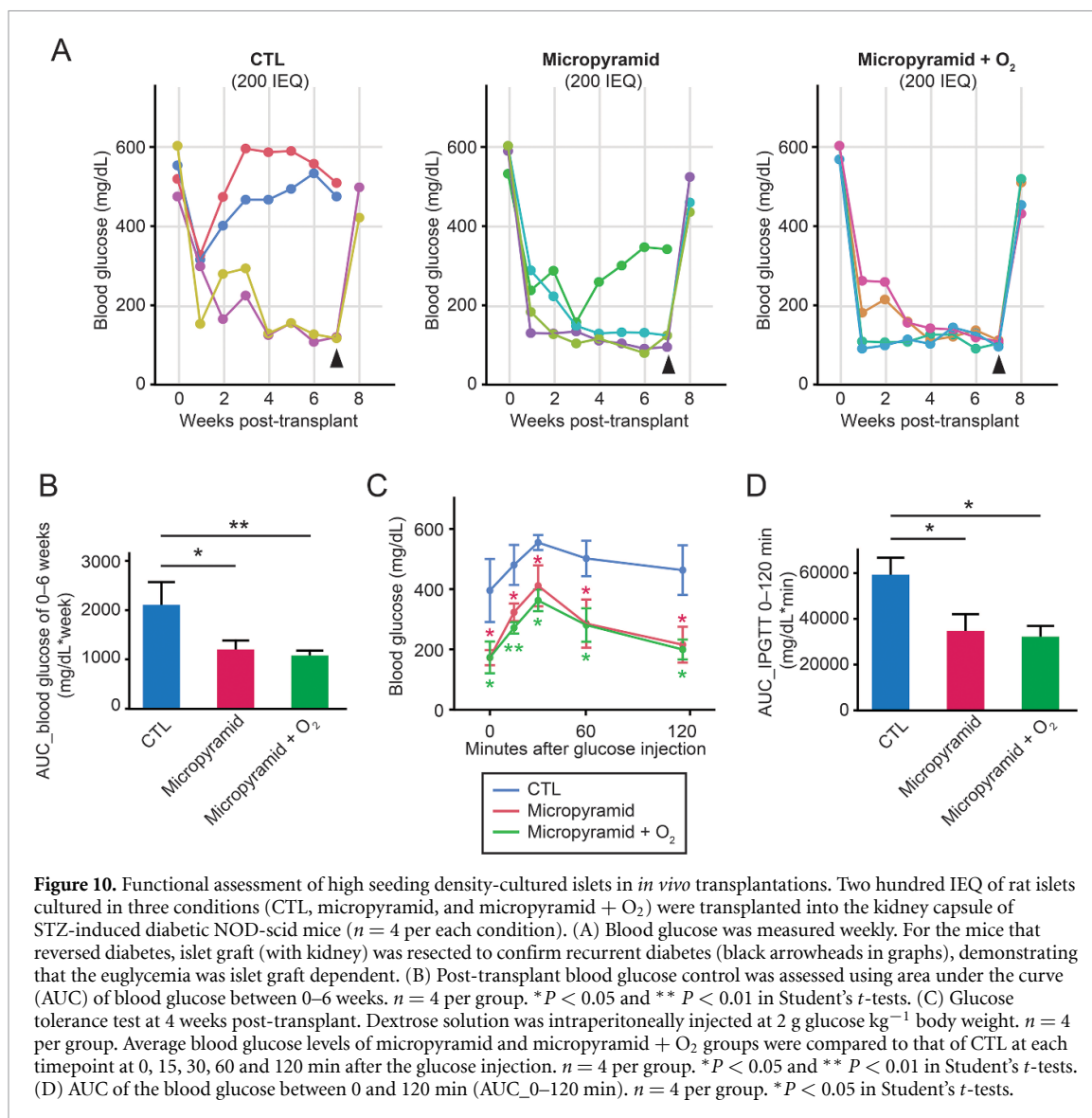
To investigate islet metabolism, we used islets isolated from luciferase-transgenic (Luc-Tg) rats [27]; bioluminescence from Luc-Tg cells correlates with ATP-based metabolism in the presence of luciferin [39, 53]. We measured the bioluminescence intensity emitted from the post-cultured islets in the dishes (figure 9(A)). Quantification of the bioluminescence revealed that the micropyramid and micropyramid + O_2 showed significantly higher metabolism over the CTL ($P = 0.0315$ (CTL vs. micropyramid), and $P = 0.0084$ (CTL vs. micropyramid + O_2); figure 9(B)). Additionally, we assessed the function of post-cultured islets by measuring the glucose-stimulated insulin secretion (figure 9(C)). Islets cultured in CTL secreted high insulin levels even in the low glucose environment and did not respond to the high glucose, indicating the islet damage [54, 55]. In contrast, islets cultured in micropyramid + O_2 showed the well-regulated insulin secretion in the low glucose environment and responded well to the high glucose solution. Islets cultured in micropyramid condition secreted insulin levels between the other two conditions. Stimulation index, the ratio of insulin secretion in high glucose/low glucose, was significantly higher in micropyramid + O_2 over other conditions ($P = 0.0087$ (CTL vs. micropyramid + O_2), and $P = 0.0099$ (micropyramid vs. micropyramid + O_2); figure 9(D)). In fact, the improved islet function demonstrated by the insulin secretion was inversely correlated to the HMGB1 release, an indicator of islet damage shown in figure 8(E).

3.8. Functional *in vivo* engraftment of cultured islets on micropyramid-patterned dish

Finally, we transplanted the high seeding density-cultured islets under the kidney capsule of NOD-scid

mice, which is a standardized method of islet quality assessment *in vivo* [56]. First, using pre-cultured islets, we determined the marginal islet number to reverse diabetes in this transplantation model (figure S6), demonstrating that 100 IEQ was sub-marginal to reverse diabetes, whereas 200 IEQ and more reversed diabetes at 100%. Accordingly, we cultured islets at a high seeding density of 500 IEQ/dish in three dish conditions (CTL, micropyramid, and micropyramid + O_2) for 4 d, then transplanted post-cultured 200 IEQ per mouse. Blood glucose level change over a 7 week-period showed the diabetes reversal rate at 50% (2/4), 75% (3/4), and 100% (4/4) in CTL, micropyramid, and micropyramid + O_2 , respectively (figure 10(A)). AUC of blood glucose levels between 0–6 weeks showed significantly better blood glucose control in both micropyramid and micropyramid + O_2 compared to the CTL (figure 10(B)). Glucose tolerance test at 4 weeks post-transplant demonstrated that islets cultured in micropyramid and micropyramid + O_2 dishes exhibited improved post-transplant function over the islets cultured in CTL (figures 10(C) and (D)). The occurrence of diabetic nephropathy, a major systemic complication of diabetes [46], was correlated to the uncontrolled diabetes in post-transplant period; transplantations of islets cultured in micropyramid and micropyramid + O_2 dishes reduced the complication, although no statistical significance was detected (figures S7(A) and (B)). This also demonstrated the improved post-cultured islet quality for the efficient engraftment in micropyramid and micropyramid + O_2 , compared to the CTL.

We further analyzed the transplantation outcomes between mice received post-cultured 200 IEQ islets shown in figure 10 and those received pre-cultured 200 IEQ islets demonstrated in figure S6. Mice that received cultured islets on the flat-bottom



dish (CTL) demonstrated significantly impaired post-transplant glycemic control compared to mice that received pre-culture islets (figures S8(A) and (B)). However, both micropyramid and micropyramid + O₂ demonstrated comparable transplantation outcomes to the pre-cultured islets. Similarly, IPGTT at 4 weeks after the transplantation exhibited no statistical difference between cultured islet groups and pre-culture islet groups, except for the cultured islets on the flat-bottom dish (CTL) (figures S8(C) and (D)).

4. Discussion

In this study, we addressed the challenge of high seeding density culture of isolated pancreatic islets using a simply structured micropyramid-patterned bottom dish. Combining the unique micropyramid array and modification of O₂-permeable bottom effectively prevented the fusion of cultured islets,

hypoxia-induced cell death and maintained islet functionality *in vitro*. Micropyramid-patterned bottom flasks could maintain pre-transplantation islet quality as well as quantity, which are critical factors for successful islet transplantations. Importantly, high-density-cultured islets using the micropyramid platform functionally engrafted and reversed diabetes when transplanted into diabetic animals, demonstrating the promise of this platform in regenerative medicine for a wide range of 3D spheroids.

While our platform is potentially applicable to multiple applications, it could readily contribute to the current clinical islet transplantation procedures for diabetes patients. We successfully cultured 500 IEQ/dish of pancreatic islets with the seeding density at ~ 260 IEQ cm⁻² in a 24-well plate. This is approximately 2–3 times higher than the seeding density of human pancreatic islets prior to the clinical islet transplantations (85–115 IEQ cm⁻²), in which islets are cultured at 15 000–20 000 IEQ in a flat-bottomed

conventional polystyrene T175 flask. T175 flask can easily be modified to micropyramid-pattern bottoms with PDMS modification, reducing the number of multiple tissue culture apparatus and the risk of contamination. Preparation of islets includes isolation from a donor pancreas, seeding islets onto ~ 50 flasks (depending on the islet yield), culturing, and collecting islets for transplantation. These steps are carefully performed in a clean condition in a GMP facility and intensely laborious work with contamination risk. Automating the culturing process is ideal but would require extensive modifications including GMP facility instruments and is costly. Therefore, our effort to lower the number of flasks with high seeding density is a practical and economical method to improve the current clinical islet transplantation process.

The main challenge in culturing 3D spheroids at high seeding density is O_2 depletion in the culture microenvironment. We addressed two distinct hypoxia mechanisms associated with the culture conditions: (a) intra-islet hypoxia and (b) O_2 depletion in the culture media, which exacerbates the O_2 microenvironment. Intra-islet hypoxia is caused by the limitation of the O_2 diffusion into the 3D spheroids as well as the high O_2 demand in the O_2 -consuming cells, resulting in the steep decrease of pO_2 within the 3D spheroids [13, 14]. O_2 depletion in the culture media occurs on a larger scale than intra-islet hypoxia. Critically, localized high islet density caused by the non-uniform islet distribution in the culture dish not only induces the localized hypoxia around the cultured islets but also increases the risk of islet fusion to form large, diffusion-limiting islets.

It has been previously demonstrated that the culture O_2 environment and islet size are the critical limiting factors in determining the viability of cultured pancreatic islets [13]; thus high O_2 culture environment reduces central necrosis via supplying more O_2 from the spheroid surface [13, 20–22]. Importantly, O_2 -permeable bottomed dish using PDMS was introduced for the culture of isolated islets [23], and this pioneering work has been extended to the enhanced production methods to culture stem cell-derived endocrine spheroids in an improved O_2 environment [57–59]. Although such O_2 strategies are requisite for supporting islets' high demand for O_2 at high seeding density, it is critically important to note that the improved O_2 on the islet surface can not completely counteract the intra-islet hypoxia, particularly in the large islets. For example, according to the previous literature [13], the viabilities of a 150 μm -islet and a 500 μm -islet under 21% O_2 culture conditions calculate 96.6% and 72.5%, respectively; however, oxygenated culture under 35% O_2 only increases the viability of a 500 μm -islet to 81.6%. In addition, using higher O_2 to complement intra-islet hypoxia could induce O_2 -mediated cell injury on the spheroid surface [13, 14]. This oxygenation paradox brings the

important implication that the fusion of islets should be avoided; thus, minimizing the risk of fusion is the critical strategy for high seeding density cultures of 3D spheroids.

Accordingly, our micropyramid-patterned, oxygen-permeable bottom dishes addressed two critical, challenging factors described above. To prevent the fusion of 3D spheroids, microwell and micropyramid patterns were initially compared to the conventional flat-bottom dish using the 3D-spherical dextran beads model. Although both micropatterns significantly improved the separation of beads compared to the flat bottom, multiple beads were occasionally observed in the microwells, which potentially can create the unsolicited fused large spheroids. The separation effect of the micropyramid pattern over flat bottom and microwell became evident in the high seeding density.

Our high seeding density platform can be used in multiple applications, including isolated pancreatic islets as well as 3D spheroids generated from single cells. Important note is that the purpose of this platform is not to grow the 3D spheroids from the single cells on it; our platform is suitable for the generated or isolated spheroids. Multiple methods can generate 3D spheroids from single cells, including bioreactors, microwells, and the hanging drop method [60]. After the spheroid formation, the subsequent high seeding density culture can be performed on our micropyramid-patterned platform.

In addition to lowering the number of flasks, another potential advantage of micropyramid over the microwell platform is the retrievability of 3D spheroids, including collecting islets post-culture. As many investigators are aware, spheroids are often trapped within the concave bottom microwells, hindering the collection of 3D spheroids. Thus, the collection step requires the flipping of culture plates or rigorous wash for retrieval, which increases the contamination risk, and is not ideal, especially when a high sterility standard is required in the clinical setting. Our micropyramid-pattern does not trap spheroids and have high retrievability with easy handling.

One important consideration to achieving uniform distribution of spheroids in micropatterned bottom dishes is the size and type of the micropatterning, which should be optimized according to the desired spheroid size. For example, a microwell may accommodate multiple spheroids if the spheroids are far smaller than the microwell diameter. However, if the microwell is smaller than the spheroids, spheroids may not fit the wells, and the separation function is lost. Therefore, the microwell platform is most effective when the individual 3D spheroid size is known and uniform. However, isolated islets have a wide range in diameter, inherently determined by the size of islets in the native pancreas [15, 61]. Further, the

3D spheroids produced in the bioreactors are generally not uniform. These biological fluctuations make the use of the standardized size of microwell difficult. However, the micropyramid-patterned bottom allows the 3D spheroids to sit not only at the intersection of four pyramid bases but also in the gutter between the two pyramids; we observed islets occasionally settled between the two pyramids, while large islets tend to sediment in the intersection of four pyramid bases. This unique feature of the micropyramid structure allows 3D spheroids of varying sizes to be cultured on the standardized size of the micropyramid array.

The micropyramid-bottomed dish also prevented islet movement during culture; this could occur due to the convection current of the culture media and mechanical vibration in the incubator. Several factors determine the convection current in the culture dishes, including the shape of the dish (e.g. round dish and square flask) and the media depth. Shallow culture media could minimize the cultured 3D spheroid movement even in the conventional flat-bottom dishes; however, reduced media would result in poor nutrient supply and concentrated waste, which is suboptimal in the high seeding density culture. Dynamic culture could enhance molecular diffusion; however, the instrument would be more complicated and expensive than static culture. Further, the media flow speed in dynamic cultures should be optimized for eliminating molecular diffusion as well as for minimizing shear stress [24, 62].

Although our study demonstrated the effectiveness of micropyramid-bottomed dishes in maintaining isolated pancreatic islets, there are several limitations in this study. First, we did not test the ultra-high density over 3-fold than the conventional culture, which can further reduce the preparatory workload mentioned above before islet transplantation. Second, we did not use a clinical grade PDMS material in this study; the use of the clinical grade PDMS could reduce cell toxicity and further improve the quality of cultured islets. Third, the study was conducted using rodent islets and not human islets. Although the hypoxia resistance of the islets between the species is not known, the results obtained using rodent islets may not directly translate into human islets in clinical applications. Fourth, we studied islet quality in a short-term period of 4 d-culture without culture media change, aligned to the current clinical islet culture period between islet isolation and transplantation. However, achieving a longer culture can provide flexibility to the transplantation schedule. In such a case, culture media should be regularly replaced, leading to islet movement; however, islets will re-settle in a similar pattern between the micropyramids as re-seeding. Thus, micropyramids will separate islets and prevent islet fusion. Lastly, for large-scale manufacturing (e.g. T175 flasks), each step should be considered carefully. Each component can be fabricated

using traditional manufacturing technologies such as plastic injection molding and reel-to-reel hot embossing to assemble into the final product using bonding methods such as ultrasonic welding. Additionally, the thin PDMS-micropyramid-membrane is soft and very elastic and, for its use in large flasks, may require a supporting structure underlying the membrane to prevent sagging.

In summary, micropyramid-patterned, O₂-permeable bottom can be a practical option for the high seeding density culture of 3D spheroids, which has simple structure modification with ease of use.

5. Conclusion

The combination strategy of a simply structured micropyramid array and modification of O₂-permeable bottom achieved high seeding density culture of isolated pancreatic islets. This simple modification can be an ideal high seeding density culture platform of 3D spheroids.

Data availability statement

All data that support the findings of this study are included within the article (and any sentry files). Additional data related to this paper may be available to researchers upon request.

Acknowledgments

We thank Sung Hee Kil, Ph D for critical reading and editing of the manuscript and Juan Carreno for the equipment preparations. Eiji Kobayashi, M D, Ph D provided Luc-Tg LEW rats.

Funding

Nora Eccles Treadwell Foundation (no Grant Number, HKo)

National Institutes of Health Grant R03DK129958-01 (HKo)

Author contributions

Conceptualization: HKo, EB

Methodology: RJM, KMS, JFB, KI, TT, NK, HKo

Investigation: RJM, KMS, JFB, NG, JR, KI, TT, NK, HKa, KO, HKo

Visualization: KMS, HKo

Supervision: YM, YCT, EB, FK, HKo

Writing—original draft: RJM, KMS, HKo

Writing—review & editing: RJM, KMS, YM, YCT, EB, HKo

Conflict of interests:

The authors declare no conflicts of interest.

ORCID iDs

Ryan J Myrick  <https://orcid.org/0000-0001-5506-5782>

Kuang-Ming Shang  <https://orcid.org/0000-0001-5065-7607>

Hirotake Komatsu  <https://orcid.org/0000-0003-0876-4809>

References

- [1] Andersen J et al 2020 Generation of functional human 3D cortico-motor assembloids *Cells* **183** 1913–29
- [2] Wang S, Matsumoto K, Lish S R, Cartagena-Rivera A X and Yamada K M 2021 Budding epithelial morphogenesis driven by cell-matrix versus cell-cell adhesion *Cell* **184** 3702–16
- [3] Bartosh T J, Ylostalo J H, Mohammadipoor A, Bazhanov N, Coble K, Claypool K, Lee R H, Choi H and Prockop D J 2010 Aggregation of human mesenchymal stromal cells (MSCs) into 3D spheroids enhances their antiinflammatory properties *Proc. Natl Acad. Sci. USA* **107** 13724–9
- [4] Chen Y Y, Silva P N, Syed A M, Sindhwani S, Rocheleau J V and Chan W C 2016 Clarifying intact 3D tissues on a microfluidic chip for high-throughput structural analysis *Proc. Natl Acad. Sci. USA* **113** 14915–20
- [5] Rebecca V W, Somasundaram R and Herlyn M 2020 Pre-clinical modeling of cutaneous melanoma *Nat. Commun.* **11** 2858
- [6] Han K et al 2020 CRISPR screens in cancer spheroids identify 3D growth-specific vulnerabilities *Nature* **580** 136–41
- [7] Friedrich J, Seidel C, Ebner R and Kunz-Schughart L A 2009 Spheroid-based drug screen: considerations and practical approach *Nat. Protocols* **4** 309–24
- [8] Barbone D, Yang T M, Morgan J R, Gaudino G and Broaddus V C 2008 Mammalian target of rapamycin contributes to the acquired apoptotic resistance of human mesothelioma multicellular spheroids *J. Biol. Chem.* **283** 13021–30
- [9] Shapiro A M, Pokrywczynska M and Ricordi C 2017 Clinical pancreatic islet transplantation *Nat. Rev. Endocrinol.* **13** 268–77
- [10] Lebreton F et al 2019 Insulin-producing organoids engineered from islet and amniotic epithelial cells to treat diabetes *Nat. Commun.* **10** 4491
- [11] Yamanaka S 2020 Pluripotent stem cell-based cell therapy-promise and challenges *Cell Stem Cell* **27** 523–31
- [12] Shweiki D, Neeman M, Itin A and Keshet E 1995 Induction of vascular endothelial growth factor expression by hypoxia and by glucose deficiency in multicell spheroids: implications for tumor angiogenesis *Proc. Natl Acad. Sci. USA* **92** 768–72
- [13] Komatsu H, Cook C, Wang C H, Medrano L, Lin H, Kandeel F, Tai Y C and Mullen Y 2017 Oxygen environment and islet size are the primary limiting factors of isolated pancreatic islet survival *PLoS One* **12** e0183780
- [14] Komatsu H, Kandeel F and Mullen Y 2018 Impact of oxygen on pancreatic islet survival *Pancreas* **47** 533–43
- [15] Ricordi C 1991 Quantitative and qualitative standards for islet isolation assessment in humans and large mammals *Pancreas* **6** 242–4
- [16] Shapiro A M, Lakey J R, Ryan E A, Korbitt G S, Toth E, Warnock G L, Kneteman N M and Rajotte R V 2000 Islet transplantation in seven patients with type 1 diabetes mellitus using a glucocorticoid-free immunosuppressive regimen *New Engl. J. Med.* **343** 230–8
- [17] Shapiro A M et al 2006 International trial of the Edmonton protocol for islet transplantation *New Engl. J. Med.* **355** 1318–30
- [18] Swauger S E, Hornung L N, Elder D A, Balamurugan A N, Vitale D S, Lin T K, Nathan J D and Abu-El-Haija M 2022 Predictors of glycemic outcomes at 1 year following pediatric total pancreatectomy with islet autotransplantation *Diabetes Care* **45** 295–302
- [19] Balzano G et al 2013 Extending indications for islet autotransplantation in pancreatic surgery *Ann. Surg.* **258** 210–8
- [20] Fraker C A, Cechin S, Alvarez-Cubela S, Echeverri F, Bernal A, Poo R, Ricordi C, Inverardi L and Dominguez-Bendala J 2013 A physiological pattern of oxygenation using perfluorocarbon-based culture devices maximizes pancreatic islet viability and enhances beta-cell function *Cell Transplant.* **22** 1723–33
- [21] Maillard E et al 2012 Perfluorocarbon emulsions prevent hypoxia of pancreatic beta-cells *Cell Transplant.* **21** 657–69
- [22] Komatsu H et al 2016 Isolated human islets require hyperoxia to maintain islet mass, metabolism, and function *Biochem. Biophys. Res. Commun.* **470** 534–8
- [23] Papas K K, Avgoustiniatos E S, Tempelman L A, Weir G C, Colton C K, Pisanía A, Rappel M J, Friberg A S, Bauer A C and Hering B J 2005 High-density culture of human islets on top of silicone rubber membranes *Transplant. Proc.* **37** 3412–4
- [24] Jun Y, Lee J, Choi S, Yang J H, Sander M, Chung S and Lee S H 2019 *In vivo*-mimicking microfluidic perfusion culture of pancreatic islet spheroids *Sci. Adv.* **5** eaax4520
- [25] Lenguito G, Chaimov D, Weitz J R, Rodriguez-Diaz R, Rawal S A, Tamayo-Garcia A, Caicedo A, Stabler C L, Buchwald P and Agarwal A 2017 Resealable, optically accessible, PDMS-free fluidic platform for *ex vivo* interrogation of pancreatic islets *Lab Chip* **17** 772–81
- [26] Zhou P et al 2016 The dynamic three-dimensional culture of islet-like clusters in decellularized liver scaffolds *Cell Tissue Res.* **365** 157–71
- [27] Hakamata Y, Murakami T and Kobayashi E 2006 “Firefly rats” as an organ/cellular source for long-term *in vivo* bioluminescent imaging *Transplantation* **81** 1179–84
- [28] Gonzalez N, Salgado M, Medrano L, Mullen Y and Komatsu H 2019 Isolated pancreatic islet yield and quality is inversely related to organ donor age in rats *Exp. Gerontol.* **128** 110739
- [29] Ito T, Itakura S, Todorov I, Rawson J, Asari S, Shintaku J, Nair I, Ferreri K, Kandeel F and Mullen Y 2010 Mesenchymal stem cell and islet co-transplantation promotes graft revascularization and function *Transplantation* **89** 1438–45
- [30] Podczek F and Newton J M 1994 A shape factor to characterize the quality of spheroids *J. Pharm. Pharmacol.* **46** 82–85
- [31] Komatsu H, Barriga A, Medrano L, Omori K, Kandeel F and Mullen Y 2017 Oxygenated thawing and rewarming alleviate rewarming injury of cryopreserved pancreatic islets *Biochem. Biophys. Res. Commun.* **486** 817–23
- [32] Komatsu H, Omori K, Parimi M, Rawson J, Kandeel F and Mullen Y 2016 Determination of islet viability using a zinc-specific fluorescent dye and a semi-automated assessment method *Cell Transplant.* **25** 1777–86
- [33] Scaffidi P, Misteli T and Bianchi M E 2002 Release of chromatin protein HMGB1 by necrotic cells triggers inflammation *Nature* **418** 191–5
- [34] Matsuoka N et al 2010 High-mobility group box 1 is involved in the initial events of early loss of transplanted islets in mice *J. Clin. Invest.* **120** 735–43
- [35] Klune J R, Dhupar R, Cardinal J, Billiar T R and Tsung A 2008 HMGB1: endogenous danger signaling *Mol. Med.* **14** 476–84
- [36] Slepchenko K G, Corbin K L and Nunemaker C S 2019 Comparing methods to normalize insulin secretion shows the process may not be needed *J. Endocrinol.* **241** 149–59
- [37] Wang L H, Ernst A U, Flanders J A, Liu W, Wang X, Datta A K, Epel B, Kotecha M, Papas K K and Ma M 2021 An inverse-breathing encapsulation system for cell delivery *Sci. Adv.* **7** eabd5835
- [38] Komatsu H, Rawson J, Barriga A, Gonzalez N, Mendez D, Li J, Omori K, Kandeel F and Mullen Y 2018 Posttransplant oxygen inhalation improves the outcome of subcutaneous

- islet transplantation: a promising clinical alternative to the conventional intrahepatic site *Am. J. Transplant.* **18** 832–42
- [39] Komatsu H, Gonzalez N, Salgado M, Cook C A, Li J, Rawson J, Omori K, Tai Y C, Kandeel F and Mullen Y 2020 A subcutaneous pancreatic islet transplantation platform using a clinically applicable, biodegradable Vicryl mesh scaffold—an experimental study *Transplant. Int.* **33** 806–18
- [40] Omori K et al 2007 Improvement of human islet cryopreservation by a p38 MAPK inhibitor *Am. J. Transplant.* **7** 1224–32
- [41] Komatsu H et al 2019 Optimizing temperature and oxygen supports long-term culture of human islets *Transplantation* **103** 299–306
- [42] Komatsu H et al 2021 A multiparametric assessment of human islets predicts transplant outcomes in diabetic mice *Cell Transplant.* **30** 9636897211052291
- [43] Salgado M, Gonzalez N, Medrano L, Rawson J, Omori K, Qi M, Al-Abdullah I, Kandeel F, Mullen Y and Komatsu H 2020 Semi-automated assessment of human islet viability predicts transplantation outcomes in a diabetic mouse model *Cell Transplant.* **29** 963689720919444
- [44] Yoshimatsu G et al 2017 Pancreatic beta-cell-derived IP-10/CXCL10 isletokine mediates early loss of graft function in islet cell transplantation *Diabetes* **66** 2857–67
- [45] Wolf G and Ziyadeh F N 1999 Molecular mechanisms of diabetic renal hypertrophy *Kidney Int.* **56** 393–405
- [46] Kato M and Natarajan R 2014 Diabetic nephropathy—emerging epigenetic mechanisms *Nat. Rev. Nephrol.* **10** 517–30
- [47] Qian Y, Feldman E, Pennathur S, Kretzler M and Brosius F C 2008 From fibrosis to sclerosis: mechanisms of glomerulosclerosis in diabetic nephropathy *Diabetes* **57** 1439–45
- [48] Giuliani M, Moritz W, Bodmer E, Dindo D, Kugelmeier P, Lehmann R, Gassmann M, Groscurth P and Weber M 2005 Central necrosis in isolated hypoxic human pancreatic islets: evidence for postisolation ischemia *Cell Transplant.* **14** 67–76
- [49] Itoh T, Takita M, SoRelle J A, Shimoda M, Sugimoto K, Chujo D, Qin H, Naziruddin B, Levy M F and Matsumoto S 2012 Correlation of released HMGB1 levels with the degree of islet damage in mice and humans and with the outcomes of islet transplantation in mice *Cell Transplant.* **21** 1371–81
- [50] Kubis H P, Hanke N, Scheibe R J and Gros G 2005 Accumulation and nuclear import of HIF1 alpha during high and low oxygen concentration in skeletal muscle cells in primary culture *Biochim. Biophys. Acta* **1745** 187–95
- [51] Sato Y, Inoue M, Yoshizawa T and Yamagata K 2014 Moderate hypoxia induces beta-cell dysfunction with HIF-1-independent gene expression changes *PLoS One* **9** e114868
- [52] Burke B, Giannoudis A, Corke K P, Gill D, Wells M, Ziegler-Heitbrock L and Lewis C E 2003 Hypoxia-induced gene expression in human macrophages: implications for ischemic tissues and hypoxia-regulated gene therapy *Am. J. Pathol.* **163** 1233–43
- [53] Nakatsu T, Ichiyama S, Hiratake J, Saldanha A, Kobashi N, Sakata K and Kato H 2006 Structural basis for the spectral difference in luciferase bioluminescence *Nature* **440** 372–6
- [54] Corkey B E, Deeny J T and Merrins M J 2021 What regulates basal insulin secretion and causes hyperinsulinemia? *Diabetes* **70** 2174–82
- [55] Graciano M F, Valle M M, Kowluru A, Curi R and Carpinelli A R 2011 Regulation of insulin secretion and reactive oxygen species production by free fatty acids in pancreatic islets *Islets* **3** 213–23
- [56] Papas K K, Suszynski T M and Colton C K 2009 Islet assessment for transplantation *Curr. Opin. Organ. Transplant.* **14** 674–82
- [57] Fraker C A, Alvarez S, Papadopoulos P, Giraldo J, Gu W, Ricordi C, Inverardi L and Dominguez-Bendala J 2007 Enhanced oxygenation promotes beta-cell differentiation *in vitro* *Stem Cells* **25** 3155–64
- [58] Cechin S, Alvarez-Cubela S, Giraldo J A, Molano R D, Villate S, Ricordi C, Pileggi A, Inverardi L, Fraker C A and Dominguez-Bendala J 2014 Influence of *in vitro* and *in vivo* oxygen modulation on beta cell differentiation from human embryonic stem cells *Stem Cells Transl. Med.* **3** 277–89
- [59] Suenaga R, Konagaya S, Yamaura J, Ito R, Tanaka S, Ishizaki Y and Toyoda T 2022 Microwell bag culture for large-scale production of homogeneous islet-like clusters *Sci. Rep.* **12** 5221
- [60] McKee C and Chaudhry G R 2017 Advances and challenges in stem cell culture *Colloids Surf. B* **159** 62–77
- [61] Komatsu H, Salgado M, Gonzalez N, Medrano L, Rawson J, Omori K, Qi M, Al-Abdullah I, Kandeel F and Mullen Y 2020 High fractions of large islets in human islet preparations detrimentally affect posttransplant outcomes in streptozotocin-induced diabetic immunodeficient mice *Pancreas* **49** 650–4
- [62] Shenkman R M, Godoy-Silva R, Papas K K and Chalmers J J 2009 Effects of energy dissipation rate on islets of Langerhans: implications for isolation and transplantation *Biotechnol. Bioeng.* **103** 413–23
- [63] Buchwald P 2009 FEM-based oxygen consumption and cell viability models for avascular pancreatic islets *Theor. Biol. Med. Model.* **6** 5
- [64] Xing W, Yin M, Lv Q, Hu Y, Liu C and Zhang J 2014 *Rotating Electrode Methods and Oxygen Reduction Electrocatalysts* (Amsterdam: Elsevier) pp 1–31
- [65] Merkel T, Bondar V, Nagai K, Freeman B and Pinnau I 2000 Gas sorption, diffusion, and permeation in poly (dimethylsiloxane) *J. Polym. Sci. B* **38** 415–34
- [66] Forstner H and Gnaiger E 1983 *Polarographic Oxygen Sensors* (Berlin: Springer) pp 321–33
- [67] Kim M-C, Lam R H, Thorsen T and Asada H H 2013 Mathematical analysis of oxygen transfer through polydimethylsiloxane membrane between double layers of cell culture channel and gas chamber in microfluidic oxygenator *Microfluid. Nanofluidics* **15** 285–96
- [68] Suszynski T M, Avgoustiniatos E S and Papas K K 2016 Oxygenation of the intraportally transplanted pancreatic islet *J. Diabetes Res.* **2016** 7625947